Journal of Power Sources 218 (2012) 280–285

Contents lists available at SciVerse ScienceDirect

Journal of Power Sources

journal homepage: www.elsevier.com/locate/jpowsour

Enhanced performance for dye-sensitized solar cells based on spherical TiO_2 nanorod-aggregate light-scattering layer

Zhao-Hui Liu, Xun-Jia Su*, Gen-Liang Hou, Song Bi, Zhou Xiao, Hai-Peng Jia

Laboratory for Advanced Materials and Technology, Xi'an Research Institute of High Technology, Xi'an, 710025, China

HIGHLIGHTS

- Spherical TiO_2 nanorod aggregates were fabricated as a light-scattering layer in dye-sensitized solar cells (DSSCs).
- They possess a large surface area for dye adsorption.
- They can generate efficient light scattering.
- They favorize long exciton lifetime.
- They exhibit improved DSSC performance.

ARTICLE INFO

Article history:
Received 28 May 2012
Received in revised form
26 June 2012
Accepted 30 June 2012
Available online 6 July 2012

Keywords:
Dye-sensitized solar cells
Bilayer-structured photoelectrode
Nanorod aggregates
Light scattering
Exciton lifetime

ABSTRACT

A new bilayer-structured photoelectrode film with spherical TiO_2 nanorod aggregates as a light-scattering overlayer and nanocrystalline TiO_2 as an underlayer is fabricated and studied with the aim of improving energy conversion efficiency in dye-sensitized solar cells (DSSCs). An overall energy conversion efficiency of 6.10% and a short-circuit photocurrent density of 18.47 mA cm^{-2} are achieved by introducing a spherical TiO_2 nanorod-aggregate light-scattering layer. These are respectively 37.1% and 42.6% higher than those of a DSSC using a conventional 200 nm-diameter solid TiO_2 particle light-scattering layer. These improvements are attributed to the spherical TiO_2 nanorod-aggregate overlayer, which has a large surface area for sufficient dye adsorption, sub-micrometer size for efficient light scattering, and lower surface state traps, allowing a longer exciton lifetime.

1. Introduction

Dye-sensitized solar cells (DSSCs) have been widely recognized as a promising alternative to conventional silicon cells since they were reported by O'Regan and Grätzel in 1991, owing to their advantages of low cost, good stability, and compatibility with flexible substrates [1–5]. One of the main distinguishing features of DSSCs is their mesoporous wide bandgap semiconductor photoelectrode, which adsorbs dye molecules onto its surface to capture the incident photons [6]. To fabricate efficient DSSCs, a large surface area and extensive light scattering are essential for obtaining a high light-harvesting efficiency from the photoelectrode films [7]. For conventional DSSCs, the mesoporous photoelectrode films composed of small-sized (usually 15–30 nm) TiO_2 nanocrystalline particles are advantageous in providing a large surface on which the sensitizer dyes are absorbed [8]. However, small nanocrystalline particles result in low-intensity Rayleigh back-scattering [9,10], giving low solar light capture by dye molecules, especially in the 600–800 nm wavelength range. Hence, an additional light-scattering layer consisting of large-sized solid particles (200–400 nm in diameter), shown in Fig. 1a, has been widely accepted to guarantee adequate light absorption in the mesoporous films by increasing the optical path length of photons and confining the incident light to within the films [11–14], thereby increasing DSSC energy conversion efficiencies. However, such large particles offer few benefits other than light scattering. The surface area is decreased by these large-sized particles, resulting in an undesired reduction in dye absorption [15,16]. It is therefore desirable to use an efficient light-scattering layer with the nanocrystalline films to prevent the loss of the necessary surface area for dye absorption.

Several groups have recently attempted to employ nanocrystalline aggregates as light-scattering particles, because their unique structures have both large surface areas and good light-

* Corresponding author. Tel.: +86 29 84744097; fax: +86 29 84741918.
E-mail address: xunjiasu@163.com (X.-J. Su).

0378-7753/$ – see front matter © 2012 Elsevier B.V. All rights reserved.
http://dx.doi.org/10.1016/j.jpowsour.2012.06.104

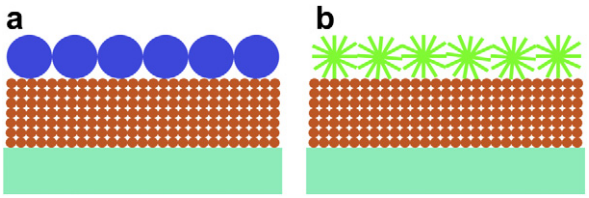

Fig. 1. Schematic of bilayer-structured photoelectrode films with different light-scattering layers: (a) large-sized solid particles; (b) spherical TiO_2 nanorod aggregates.

scattering ability [15–20]. A bilayer photoelectrode film with a nanocrystalline TiO_2 underlayer and nano-embossed hollow-sphere TiO_2 aggregate overlayer efficiently generating photo-excited electrons, had good light-scattering properties, and high energy conversion efficiency [16]. A bilayer photoelectrode film with mesoporous TiO_2 aggregates as the light-scattering layer showed a 12.3% higher efficiency than a bilayer photoelectrode film with 400 nm-diameter solid particles as the light-scattering layer [18], suggesting that the mesoporous aggregates might show both additional dye adsorption and efficient light scattering.

Because of the interesting performance of nanocrystalline aggregates, we report here the use of spherical TiO_2 nanorod aggregates (NR-TiO_2) with multiple functions as the light-scattering layer (Fig. 1b) in the bilayer-structured photoelectrode with a nanocrystalline TiO_2 (NC-TiO_2) underlayer. The enhanced performance of such a bilayer-structured photoelectrode for DSSCs was studied in comparison with the conventional bilayer-structured photoelectrode using commercial 200 nm-diameter solid TiO_2 particles (SP-TiO_2) as a light-scattering layer.

2. Experimental

2.1. Preparation of spherical TiO_2 nanorod aggregates

All the chemicals studied in the experiments were analytical grade and were used without any further purification. The NR-TiO_2 was synthesized via a facile hydrothermal method. In a typical synthesis [21], 5 mL of titanium trichloride ($TiCl_3$, 15 wt%) was dissolved in 30 mL of water, and then supersaturated NaCl was added. After stirring for 10 min at room temperature, the aqueous solution was transferred to a 50 mL Teflon-lined stainless steel autoclave and maintained in an electric oven at 160 °C for 2 h. After cooling naturally to room temperature, the white precipitate was separated via centrifugation and then washed thoroughly with deionized water and ethanol. The wet NR-TiO_2 obtained was used to prepare NR-TiO_2 paste.

2.2. Fabrication of DSSCs

The NR-TiO_2 paste was prepared by the following procedure. The wet NR-TiO_2 powders were directly mixed with 8 g α-terpineol and 10 g of 10 wt% solution of ethyl cellulose in ethanol in a mortar grinder, then ground for 1 h. Finally, the mixture was stirred with a magnetic bar until a highly viscous paste formed. For comparison, the SP-TiO_2 (Heptachroma, Dalian, China) paste and the NC-TiO_2 (P25, Degussa, Frankfurt am Main, Germany) paste were prepared by a similar procedure to that for the NR-TiO_2 paste. The latter was coated.

The TiO_2 paste was coated onto the fluorine-doped tin-oxide-coated glasses (FTO, NSG Group, Tokyo, Japan) using the doctor-blade method. Prior to the fabrication of TiO_2 films, the FTO glass supports were ultrasonically cleaned sequentially in chloroform, acetone and water each for 30 min. The NC-TiO_2 paste was then deposited onto the FTO glass support by using a doctor-blade technique and was then baked over an alcohol burner for 1 min to obtain an underlayer. Using a similar procedure, the as-prepared NR-TiO_2 and SP-TiO_2 pastes were deposited on the NC-TiO_2 underlayer to form bilayer-structured films respectively. The bilayer-structured films were subsequently heated at 450 °C for 30 min. Thicknesses of the layers are given in Section 3.1, below. The films were then immersed in a 40 mM aqueous $TiCl_4$ solution at 70 °C for 30 min, rinsed with water and ethanol, and sintered at 500 °C for 30 min. After cooling to 80 °C, the bilayer-structured films were immersed in a 0.5 mM N719 dye [cis-bis(isothiocyanato)-bis(2,2′-bipyridyl-4,4′-dicarboxylato)-ruthenium(II)bis-tetrabutylammonium, Solaronix SA, Aubonne, Switzerland] solution in anhydrous ethanol and kept at room temperature for 20–24 h to assure complete sensitizer uptake. The photoelectrodes obtained were then rinsed with ethanol to remove the additional dye. Counter-electrodes were fabricated by depositing a transparent platinum thin film on FTO substrates from H_2PtCl_6 isopropanol solution using a spin-coating and pyrolyzing method. The redox electrolyte used was 0.5 M LiI, 0.05 M I_2, 0.3 M 1,2-dimethyl-3-propylimidazolium iodide, and 0.5 M 4-tert-butylpyridine in acetonitrile. The two electrodes were sealed together with a hot-melt polymer film (Surlyn 1702, DuPont, Wilmington, USA). The active area of the resulting cells exposed to light was approximately 0.36 cm^2 (0.6 cm × 0.6 cm).

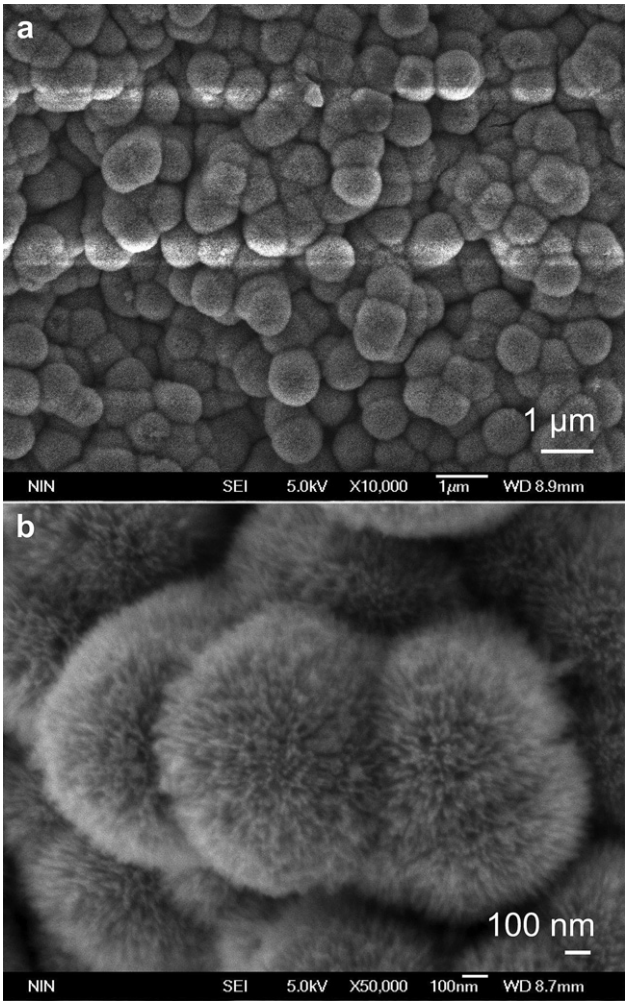

Fig. 2. SEM image (a) and (b) high-magnification image of spherical TiO_2 nanorod aggregates.

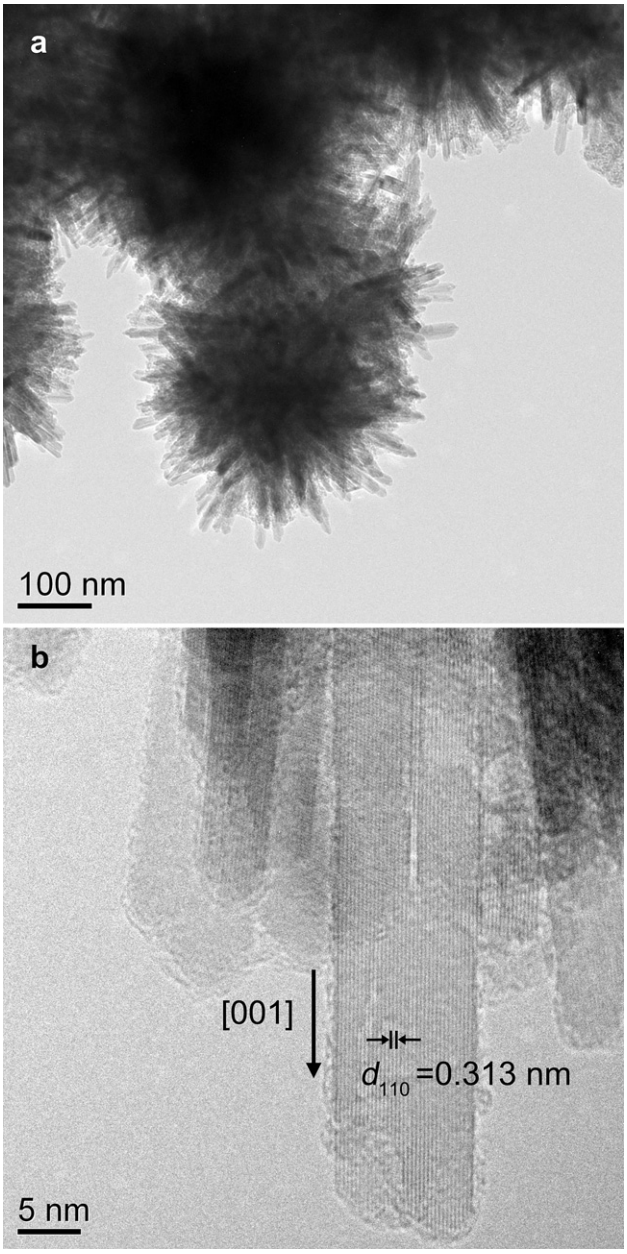

Fig. 3. (a) TEM image of spherical TiO_2 nanorod aggregates; (b) HRTEM image of nanorods in spherical TiO_2 nanorod aggregates.

2.3. Characterization

The morphologies of samples were examined by field emission scanning electron microscopy (FESEM, JSM-6700F, JEOL, Tokyo, Japan) and transmission electron microscopy (TEM, JEM-3010, JEOL, Tokyo, Japan). Phase identification was conducted by X-ray diffraction (XRD, D8 ADVANCE, BRUKER AXS, Karlsruhe, Germany). The surface area of the NR-TiO_2 was determined by a Brunauer–Emmett–Teller (BET) N_2 gas adsorption/desorption apparatus (ASAP2000, Micromeritics, Atlanta, USA). The amounts of absorbed dye were measured by desorbing the dye from the dye-sensitized films in a 0.1 M NaOH solution in water and ethanol (1:1, v/v), and then the concentration of desorbed dye in the NaOH solution was measured using an UV–visible–NIR spectrophotometer (Lambda 950, PerkinElmer, Waltham, USA) [22]. The reflectance spectra of the undyed and dyed films were measured using the same spectrophotometer equipped with an integrating sphere assembly. The photocurrent–voltage characteristics and open-circuit voltage decay (OCVD) of solar cells were recorded by CHI 660C workstation (Chenhua, Shanghai, China) under simulated AM 1.5 sunlight illumination with a light output of 100 mW cm^{-2}. The light source was a 500 W Xe lamp (Changtuo, Beijing, China) coupled with an AM 1.5G filter.

3. Results and discussion

3.1. Characterization of the spherical TiO_2 nanorod aggregates

Fig. 2a is a typical SEM image of the as-prepared NR-TiO_2, indicating that the diameters of the monodispersed NR-TiO_2 are in the range of 200–400 nm. Closer observation (Fig. 2b) reveals that the NR-TiO_2 is composed of numerous uniform radial nanorods, whose diameters and lengths are about 10 and 150 nm respectively. The corresponding TEM image (Fig. 3a) further confirms that all of the NR-TiO_2 consists of uniform nanorods, and this unique structure is favorable for obtaining high surface area. The surface area of the NR-TiO_2 determined by the BET method is 109 $m^2\ g^{-1}$, which is much higher than that of NC-TiO_2 (51 $m^2\ g^{-1}$). Further examination of the nanorods with HRTEM (Fig. 3b) shows that they are single crystals, completely crystalline along their entire length. A (110) interplanar distance of 0.313 nm is clearly observed, consistent with the rutile phase (PDF# 21-1276), and this is further confirmed by the XRD patterns (Fig. 4). The nanorods grow along the (110) crystal plane with a preferred [001] orientation, since the Cl^{-1} ions in the hydrothermal solution preferentially adsorb on the (110) surfaces and retard their growth rates [23].

3.2. Photovoltaic performance of DSSCs

To investigate the effect of the NR-TiO_2 light-scattering layer on the photovoltaic properties of DSSCs, bilayer-structured photoelectrodes made from NC-TiO_2 underlayers with different light-scattering NR-TiO_2 and SP-TiO_2 overlayers were prepared using a similar procedure, and the corresponding samples were denoted as NR-NC and SP-NC respectively. Fig. 5 shows the SEM images of the NR-NC, showing that the total thickness of the NR-NC film is about 12 μm and the thickness of the NR-TiO_2 overlayer is about 4 μm. Fig. 6 shows the photocurrent–voltage (J–V) curves of the three cells, and the results are summarized in Table 1. The cell based on the NR-NC photoelectrode shows a short-circuit photocurrent density (J_{sc}) 1.5 times higher and slightly higher open-circuit voltage (V_{oc}), compared with the cell based on the SP-NC photoelectrode. In

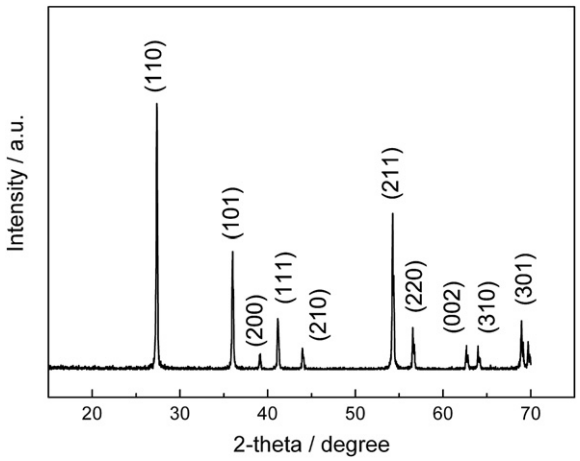

Fig. 4. X-ray diffraction pattern of spherical TiO_2 nanorod aggregates.

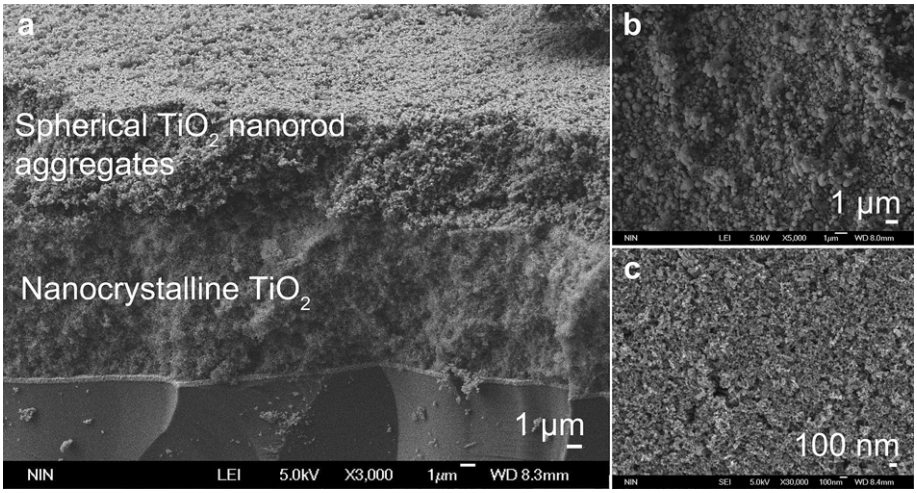

Fig. 5. (a) Cross-sectional SEM image of a bilayer-structured film showing the nanocrystalline TiO_2 underlayer and the spherical TiO_2 nanorod-aggregate overlayer; surface SEM images for (b) spherical TiO_2 nanorod-aggregate overlayer and (c) nanocrystalline TiO_2 underlayer.

comparison with pure NC-TiO_2, the NR-NC shows a 64% increment in J_{sc} and slightly lower V_{oc}. As a result, the energy conversion efficiency of the NR-NC is the highest of the three cells. The much higher J_{sc} is probably related to either the amount of dye adsorbed, or light scattering, or both. The adsorbed amounts of N719 dye were determined by measuring the eluted dye concentration from the porous TiO_2 films using UV–visible absorption spectroscopy. As shown in Table 1, the NR-NC exhibits 1.2 times more dye absorption compared to the SP-NC, and therefore the much higher J_{sc} observed for the NR-NC compared to the SP-NC is mainly attributed to the larger amount of dye adsorbed on the NR-TiO_2. However, it should be noted that the NR-NC also shows a higher J_{sc} than pure NC-TiO_2 in spite of the fact that the amount of dye adsorbed by the NR-NC is 8% lower than that adsorbed by pure NC-TiO_2. This might be due to a difference in light-scattering efficiency.

3.3. Light-scattering ability of spherical TiO_2 nanorod aggregates

To investigate the light-scattering efficiency in detail, the reflectance of each film was studied. Fig. 7 shows the UV–visible reflectance spectra of the films derived from the NR-NC with and without N719 dye, as well as those consisting of the SP-NC and pure NC-TiO_2. As shown in Fig. 7a, the NR-NC and SP-NC films have similar reflectance in the 400–800 nm regions, which is much higher than that of pure NC-TiO_2, indicating that the former two films have better light-scattering ability due to their larger particle size, which is comparable to the wavelength of white light [24]. Fig. 7b shows the reflectance spectra of the above dye-adsorbed films. After dye loading, the reflectance of the above three films decreases drastically in the short wavelength range of 400–600 nm, which is mainly due to light absorption by the dye molecules. Furthermore, the dye-adsorbed NR-NC film has a similar reflectance to that of dye-adsorbed pure NC-TiO_2 film in the short wavelength range (400–600 nm), but it shows a much higher reflectance than that of the dye-adsorbed pure NC-TiO_2 film in the long wavelength region, comparable to that of the dye-adsorbed SP-NC film. As the N719 dye molecules used show poor solar light absorption ability in the 600–800 nm long wavelength range, a higher reflectance dye-adsorbed film in this range indicates a better light-scattering ability [16]. Therefore, the light-scattering efficiency of the NR-NC film is similar to that of the SP-NC film, but is much higher than that of the pure NC-TiO_2 film. Thus its higher J_{sc} results from its superior light-scattering efficiency.

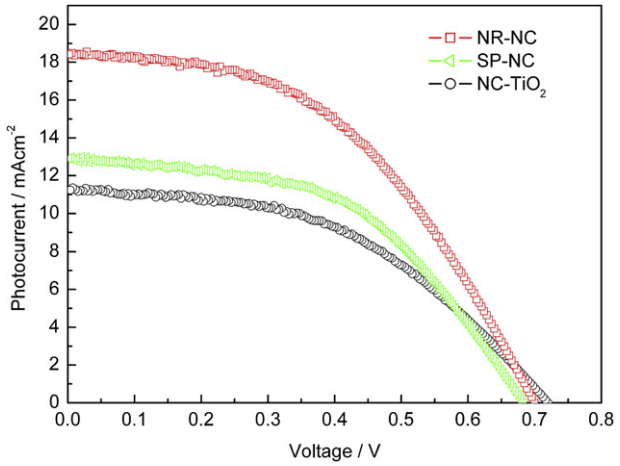

Fig. 6. Photocurrent–voltage curves of the DSSCs based on NR-NC, SP-NC, and pure NC-TiO_2 films.

3.4. Open-circuit voltage decay (OCVD) measurement

The OCVD technique has been employed as a powerful tool to study interfacial recombination processes in the TiO_2 DSSCs between photoinjected electrons and the electrolyte in the dark [25–27]. It can provide some quantitative information on the electron recombination rate. Fig. 8a shows the OCVD decay curves of the cells derived from the NR-NC and SP-NC films. It is seen that the OCVD response of the cell with the NR-NC film was much slower than that of the cell using the SP-NC film. Since the decay of the V_{oc} reflects the decrease in the electron concentration, which is mainly caused by the charge recombination [25], the cell using the NR-NC film has a lower electron recombination rate than that of the cell using the SP-NC film. Under the present open-circuit and dark state conditions, the exciton lifetime (τ_n) in DSSCs can change with the cell's V_{oc} due to the shift of the semiconductor Fermi level [26]. Thus the effects of the electron traps on the recombination reaction can be qualitatively explained by analyzing the change of τ_n–V_{oc} relation curves. τ_n was calculated with the OCVD results in Fig. 8a according to the following equation [28]:

$$\tau_n = -\frac{k_B T}{e}\left(\frac{dV_{oc}}{dt}\right)^{-1} \quad (1)$$

Table 1
Summarized performance of the DSSCs based on NR-NC, SP-NC, and pure NC-TiO_2 films.

Samples	J_{sc} (mA cm^{-2})	V_{oc} (V)	FF	η (%)	Thickness (μm)	Adsorbed dye ($\times 10^{-8}$ mol cm^{-2})
NR-NC	18.47	0.70	0.47	6.10	12.0	12.07
SP-NC	12.95	0.68	0.51	4.45	11.8	10.37
NC-TiO_2	11.28	0.72	0.48	3.82	12.3	13.16

where k_B is the Boltzmann constant, T is absolute temperature, e is the electronic charge, and dV_{oc}/dt is the derivative of the transient open-circuit voltage.

Fig. 8b shows the τ_n–V_{oc} relation curves of cells made from the NR-NC and SP-NC films. It can be clearly seen that the exciton lifetime (τ_n) shows an exponential dependence on the V_{oc}, and at any given V_{oc} the exciton lifetime (τ_n) of the cell based on the NR-NC film is longer than that of the cell based on the SP-NC film. According to Zaban's model, the exciton lifetime is mainly affected by the surface state traps in mesoporous TiO_2 films [29]. Since the NR-NC and SP-NC photoelectrodes have the same NC-TiO_2 underlayers, one may conclude that the NR-TiO_2 overlayer has fewer surface state traps. It has been reported that TiO_2 nanorods have better electron transport ability than TiO_2 particles due to the presence of fewer surface state traps [30–32]. For the SP-NC, increased grain boundaries may increase surface state traps, and thus reduce the exciton lifetime, resulting in relatively low photocurrent and efficiency. Therefore, use of the NR-TiO_2 as a light-scattering layer is also favorable for prolonging the exciton lifetime and reducing the photoelectron recombination.

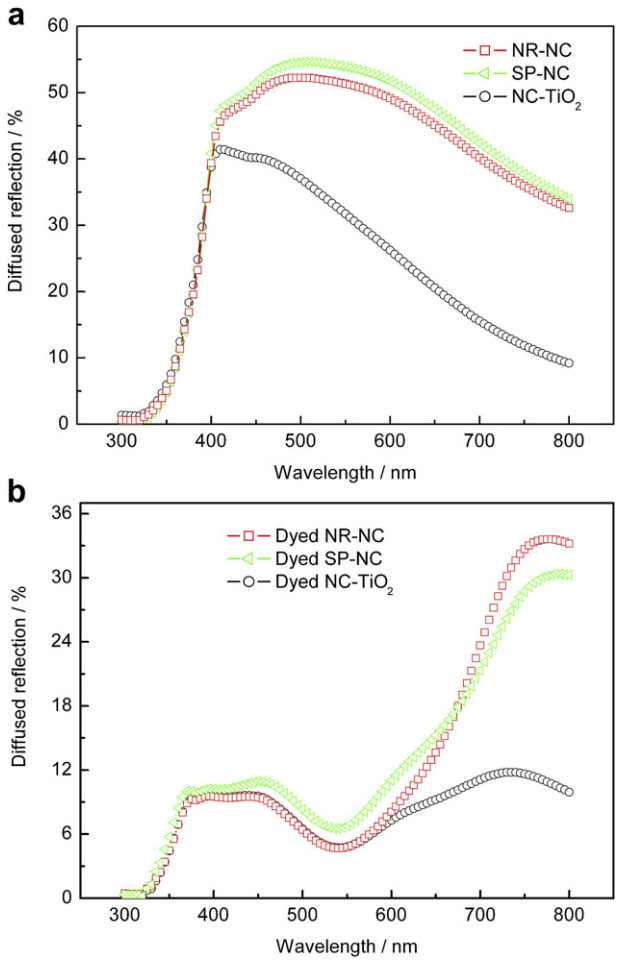

Fig. 7. Diffused reflectance spectra of the NR-NC, SP-NC, and pure NC-TiO_2 films (a) without and (b) with adsorbed N719 dye.

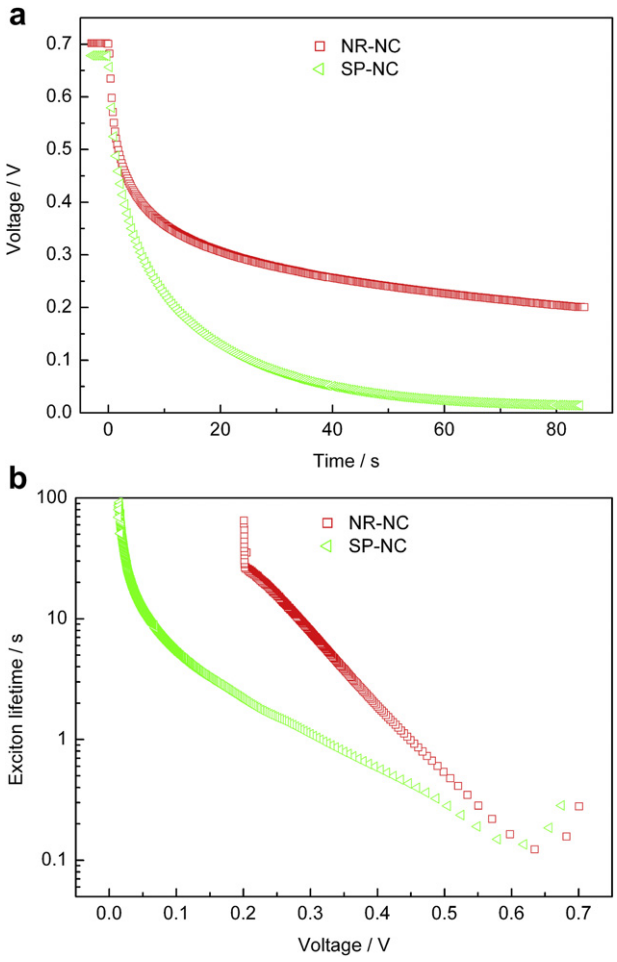

Fig. 8. (a) Open-circuit voltage decay curves of the DSSCs with NR-NC and SP-NC films; (b) exciton lifetime as a function of open-circuit voltage of DSSCs with NR-NC and SP-NC films.

4. Conclusions

Bilayer-structured photoelectrode films derived from spherical TiO_2 nanorod-aggregate overlayers and nanocrystalline TiO_2 underlayers were fabricated and the effect of spherical TiO_2 nanorod-aggregate light-scattering layers on the performance of DSSCs was investigated. Spherical TiO_2 nanorod aggregates with high surface area used as the light-scattering layer not only enhanced light scattering without sacrificing accessible surface area for dye adsorption, but also prolonged exciton lifetime. Compared with the traditional DSSCs with 200 nm-diameter solid TiO_2 particles as the light-scattering layer, the energy conversion efficiency and short-circuit photocurrent density of DSSCs using spherical TiO_2 nanorod aggregates as the light-scattering layer were improved by 37.1% and 42.6% respectively.

References

[1] B. O'Regan, M. Grätzel, Nature 353 (1991) 737–740.
[2] M. Grätzel, Nature 414 (2001) 338–344.
[3] M.K. Nazeeruddin, A. Kay, I. Rodicio, R.H. Baker, E. Müller, P. Liska, N. Vlachopoulos, M. Grätzel, J. Am. Chem. Soc. 115 (1993) 6382–6390.
[4] P. Wang, S.M. Zakeeruddin, J.E. Moser, M.K. Nazeeruddin, T. Sekiguchi, M. Grätzel, Nat. Mater. 2 (2003) 402–407.

[5] D.B. Kuang, C. Klein, S. Ito, J.E. Moser, R. Humphry-Baker, N. Evans, F. Duriaux, C. Grätzel, S.M. Zakeeruddin, M. Grätzel, Adv. Mater. 19 (2007) 1133–1137.
[6] A. Hagfeldt, G. Boschloo, L.C. Sun, L. Kloo, H. Pettersson, Chem. Rev. 110 (2010) 6595–6663.
[7] L.M. Peter, J. Phys. Chem. Lett. 2 (2011) 1861–1867.
[8] Q.F. Zhang, G.Z. Cao, Nano Today 6 (2011) 91–109.
[9] A. Usami, Sol. Energy Mater. Sol. Cells 62 (2000) 239–246.
[10] S. Hore, P. Nitz, C. Vetter, C. Prahl, M. Niggemann, R. Kern, Chem. Commun. 15 (2005) 2011–2013.
[11] Y.C. Qiu, W. Chen, S.H. Yang, Angew. Chem., Int. Ed. 49 (2010) 3675–3679.
[12] L. Yang, Y. Lin, J.G. Jia, X.R. Xiao, X.P. Li, X.W. Zhou, J. Power Sources 182 (2008) 370–376.
[13] S. Ito, T.N. Murakami, P. Comte, P. Liska, C. Grätzel, M.K. Nazeeruddin, M. Grätzel, Thin Solid Films 516 (2008) 4613–4619.
[14] Q.Q. Miao, L.Q. Wu, J.N. Cui, M.D. Huang, T.L. Ma, Adv. Mater. 23 (2011) 2764–2768.
[15] J.T. Xia, Q.F. Zhang, K. Parka, Y.M. Sun, G.Z. Cao, Electrochim. Acta 56 (2011) 1960–1966.
[16] H.J. Koo, Y.J. Kim, Y.H. Lee, W.I. Lee, K. Kim, N.G. Park, Adv. Mater. 20 (2008) 195–199.
[17] K. Yan, Y. Qiu, W. Chen, M. Zhang, S. Yang, Energy Environ. Sci. 4 (2011) 2168–2176.
[18] F.Z. Huang, D.H. Chen, X.L. Zhang, R.A. Caruso, Y.B. Cheng, Adv. Funct. Mater. 20 (2010) 1301–1305.
[19] S.H. Jang, Y.J. Kim, H.J. Kim, W. Lee, Electrochem. Commun. 12 (2010) 1283–1286.
[20] Q.F. Zhang, K. Park, J.T. Xi, D. Myers, G.Z. Cao, Adv. Energy Mater. 1 (2011) 988–1001.
[21] X.L. Bai, B. Xie, N. Pan, X.P. Wang, H.Q. Wang, J. Solid State Chem. 181 (2008) 450–456.
[22] Z.S. Wang, H. Kawauchi, T. Kashima, H. Arakawa, Coord. Chem. Rev. 248 (2004) 1381–1389.
[23] B. Liu, E.S. Aydil, J. Am. Chem. Soc. 131 (2009) 3985–3990.
[24] W. Shao, F. Gu, Ch.Z. Li, M.K. Lu, Ind. Eng. Chem. Res. 49 (2010) 9111–9116.
[25] H. Yua, S.Q. Zhang, H.J. Zhao, G. Willb, P. Liu, Electrochim. Acta 54 (2009) 1319–1324.
[26] J. Bisquert, A. Zaban, M. Greenshtein, I. Mora-Sero, J. Am. Chem. Soc. 126 (2004) 13550–13559.
[27] K. Fan, W. Zhang, T.Y. Peng, J.N. Chen, F. Yang, J. Phys. Chem. C 115 (2011) 17213–17219.
[28] A. Zaban, M. Greenshtein, J. Bisquert, ChemPhysChem 4 (2003) 859–864.
[29] R. Kern, R. Sastrawan, J. Ferber, R. Stangl, J. Luther, Electrochim. Acta 47 (2002) 4213–4225.
[30] X.J. Feng, K. Shankar, O.K. Varghese, M. Paulose, T.J. Latempa, C.A. Grimes, Nano Lett. 8 (2008) 3781–3786.
[31] N.G. Park, J. Lagemaat, A.J. Frank, J. Phys. Chem. B 104 (2000) 8989–8994.
[32] R.H. Tao, J.M. Wu, H.X. Xue, X.M. Song, X. Pan, X.Q. Fang, X.D. Fang, S.Y. Dai, J. Power Sources 195 (2010) 2989–2995.